A&A 491, 889–897 (2008)
DOI: 10.1051/0004-6361:200810625

Astronomy & Astrophysics

Transiting exoplanets from the *CoRoT* space mission⋆,⋆⋆

VI. CoRoT-Exo-3b: the first secure inhabitant of the brown-dwarf desert

M. Deleuil[1], H. J. Deeg[2], R. Alonso[1], F. Bouchy[3], D. Rouan[4], M. Auvergne[4], A. Baglin[4], S. Aigrain[5], J. M. Almenara[2], M. Barbieri[1], P. Barge[1], H. Bruntt[6], P. Bordé[7], A. Collier Cameron[8], Sz. Csizmadia[9], R. De la Reza[10], R. Dvorak[11], A. Erikson[9], M. Fridlund[12], D. Gandolfi[13], M. Gillon[14], E. Guenther[13], T. Guillot[15], A. Hatzes[13], G. Hébrard[3], L. Jorda[1], H. Lammer[16], A. Léger[7], A. Llebaria[1], B. Loeillet[1,3], M. Mayor[14], T. Mazeh[17], C. Moutou[1], M. Ollivier[7], M. Pätzold[18], F. Pont[5], D. Queloz[14], H. Rauer[9,19], J. Schneider[20], A. Shporer[17], G. Wuchterl[13], and S. Zucker[17]

(Affiliations can be found after the references)

Received 16 July 2008 / Accepted 22 September 2008

ABSTRACT

Context. The *CoRoT* space mission routinely provides high-precision photometric measurements of thousands of stars that have been continuously observed for months.
Aims. The discovery and characterization of the first very massive transiting planetary companion with a short orbital period is reported.
Methods. A series of 34 transits was detected in the *CoRoT* light curve of an F3V star, observed from May to October 2007 for 152 days. The radius was accurately determined and the mass derived for this new transiting, thanks to the combined analysis of the light curve and complementary ground-based observations: high-precision radial-velocity measurements, on-off photometry, and high signal-to-noise spectroscopic observations.
Results. CoRoT-Exo-3b has a radius of 1.01 ± 0.07 $R_{\rm Jup}$ and transits around its F3-type primary every 4.26 days in a synchronous orbit. Its mass of 21.66 ± 1.0 $M_{\rm Jup}$, density of 26.4 ±5.6 g cm^{-3}, and surface gravity of $\log g = 4.72$ clearly distinguish it from the regular close-in planet population, making it the most intriguing transiting substellar object discovered so far.
Conclusions. With the current data, the nature of CoRoT-Exo-3b is ambiguous, as it could either be a low-mass brown-dwarf or a member of a new class of "superplanets". Its discovery may help constrain the evolution of close-in planets and brown-dwarfs better. Finally, CoRoT-Exo-3b confirms the trend that massive transiting giant planets ($M \geq 4\ M_{\rm Jup}$) are found preferentially around more massive stars than the Sun.

Key words. stars: planetary systems – stars: low-mass, brown-dwarfs – Sun: fundamental parameters

1. Introduction

Massive close-in planets are nowadays the most accessible population of extrasolar planets, and they are extensively being studied with both radial velocity and transit surveys. To date, the more than forty extrasolar transiting planets with known mass and radius indeed belong to this population. However, the ever increasing number of discovered new members of this group widens the range of their properties and challenges our understanding of their formation and structure.

As demonstrated by its first results (Barge et al. 2008; Alonso et al. 2008), the space mission *CoRoT* is particularly well-suited to making significant breakthroughs in our knowledge of this population of planets in short orbital periods. The instrument is performing wide-field, relative stellar photometry at ultra-high precision. It can monitor up to 12 000 stars simultaneously per observing run, over a temporal span up to 150 days of nearly continuous observations. It is thus sensitive to detecting planets with orbital periods less than 75 days. One advantage of CoRoT's performance is that it nicely matches that of ground-based radial velocity facilities. Combining the ultra-precise stellar photometry with precise radial velocity observations enable us to fully investigate the nature of the discovered objects.

We report in this paper the discovery by *CoRoT* of the smallest close-in transiting substellar object detected so far by photometry. The analysis of the high-quality *CoRoT* light curve, combined with follow-up observations, allow us to fully characterize this new intriguing object. It orbits in 4.25680 days an F-type dwarf with solar metallicity. From the derived mass we know that this object is located in the so-called brown-dwarf desert. This is the gap in the mass function that separates stellar and planetary objects.

2. *CoRoT* observations

2.1. Light curve

CoRoT-Exo-3 was observed during the first long observing run of *CoRoT* (*LRc01*) which took place from May 26th to October 25th, 2007. This stellar field is centered at $\alpha = 19^{\rm h}23^{\rm m}$, $\delta = \delta = +00°27'$ in a direction close to the Galaxy center. With a magnitude of $r' = 13.1$ (Table 1), the host star is among the brightest *CoRoT* targets, which are typically in the range 11

⋆ The *CoRoT* space mission, launched on December 27th 2006, has been developed and is operating by CNES, with the contribution of Austria, Belgium, Brasil, ESA, Germany and Spain. The first *CoRoT* data will be available to the public in February 2009 from the *CoRoT* archive: http://idoc-corot.ias.u-psud.fr/

⋆⋆ Table of the COROT photometry is only available in electronic form at the CDS via anonymous ftp to cdsarc.u-strasbg.fr (130.79.128.5) or via http://cdsweb.u-strasbg.fr/cgi-bin/qcat?J/A+A/491/889

Table 1. CoRoT-Exo-3 IDs, coordinates and magnitudes with errors.

CoRoT ID	101 368 192	
USNO-A2	0900-15209129	
2MASS	19281326+0007185	
GSC2.3	N1MO000645	
RA (2000)	19:28:13.26	
Dec (2000)	00:07:18.7	
B-mag$^{(a)}$	14.199	0.04
V-mag$^{(a)}$	13.292	0.02
r'-mag$^{(a)}$	13.099	0.01
i'-mag$^{(a)}$	12.676	0.01
$J^{(b)}$	11.936	0.028
$H^{(b)}$	11.710	0.041
$K_s{}^{(b)}$	11.618	0.033
$\mu_\alpha{}^{(c)}$	–10.8	5.6″/yr
$\mu_\delta{}^{(c)}$	–10.8	5.6″/yr

$^{(a)}$ Provided by *Exo-Dat*, based on observations taken at the *INT* telescope; $^{(b)}$ from *2-MASS* catalog; $^{(c)}$ from *UCAC2* catalog.

to 16 in r'. It is one of the targets identified as a planetary candidate in the so-called *"alarm mode"* (Quentin et al. 2006; Surace et al. 2008). Following this detection, on August 3, 2007 the time sampling of the light curve was switched from 512 s, corresponding to the co-addition on-board of 16 elementary exposures, to the nominal 32 s. As a whole, the light curve consists of 236 999 measurements with a time sampling of 512 s for the first two months, and then 32 s sampling until the end of the observational run. The data presented in this paper were reduced with the very first version of the *CoRoT* calibration pipeline (Auvergne et al., in preparation). This current version of the pipeline includes (i) the correction for the CCD zero offset and gain; (ii) the correction for the background contribution, which is done using reference photometric windows; and (iii) the correction for the satellite orbital effects. In addition, the pipeline flags outliers due to impacts of charged particles. The flux of highly energetic particles increases dramatically during the crossing of the South Atlantic Anomaly (SAA) and, despite the shielding of the focal plane, makes photometric measurements impossible. The corresponding portions of the light curve were simply removed from the final light curve. This results in a duty cycle of about 88%.

In a final step, we also corrected the light curve from the signatures of pixel defects, often called "hot-pixels". These hot-pixels are a direct consequence of high energy particle impacts onto the *CoRoT* CCD (see Pinheiro da Silva et al. 2008) and cause discontinuities in the light curve at the time of their creation. Different kinds of discontinuities are observed: a sudden increase of the apparent flux of the light curve with an exponential decay or a step-like discontinuity. We corrected these temporal signatures, case by case, by an exponential function with a time constant or a simple step function. The resulting light curve is shown in Fig. 1. We note a gradual decrease of the signal of about 2%, a behavior observed in all the *CoRoT* light curves and whose origin is ascribed to CCD aging. The S/N per 512 s, estimated on out of transit sections of the light curve, is ≃1915.

When analyzing *CoRoT* data, special care should be taken to account for the possible contamination of the target's signal by nearby stars whose Point Spread Function (PSF) falls within the quite large aperture mask of *CoRoT*. We checked in the *Exo-Dat* database (Deleuil et al., submitted) the vicinity of the target (see Sect. 3.1). *Exo-Dat* is the *CoRoT*/Exoplanet Scientific database which was used to build the Exoplanet input catalog and gathers all information on the target stars as well as their environment. Among all the stars whose flux could contribute to the light curve, the brightest one is 2.8 mag fainter in the r'-band and located at 5.6″ to the South. To evaluate the contribution of this and further nearby stars we followed the method described in Alonso et al. (2008), which gives us a value of about 8%. To properly remove its contribution to the white light curve, we identified in *Exo-Dat* a set of a dozen of stars with similar magnitude to the contaminant, observed by *CoRoT* during the same run and on the same CCD. We checked that these stars were not affected by nearby contaminants so that their light curve could be used as reference. We computed the median value of the light curves of these stars and found a fractional flux of 0.082 ± 0.007. This value was then subtracted from the light curve.

2.2. Transit parameters

A total of 34 transits are visible in the light curve, 18 belonging to the 32 s sampling part (Fig. 1). In itself, the light curve does not exhibit strong photometric variations, indicating a non-active star. The transit was analyzed using the same methodology as presented in Alonso et al. (2008), though the very low activity level of the star facilitates the analysis. We simply recall here the main steps of the method. From the series of transits, both the orbital period and the transit epoch were derived by a trapezoidal fitting to all the transit centers. The light curve was phase-folded to this ephemeris after first performing a local linear fit to the region centered around the transit in order to correct for any local variation of the light curve over a range from ±0.02 to ±0.04 in phase. The transit light curve shown in Fig. 2 was binned by 1.5×10^{-3} in phase and the error bar of each individual bin calculated as the dispersion of the points inside the bin, divided by the square root of the number of points per bin. The system parameters were then estimated by a χ^2 fitting method, following the formalism of Giménez (2006). Basically, the model is a 6-free parameters model: the transit center, the orbital phase at first contact between planet and star, the ratio of the planet to star radii, $R_p/R_\star$, the orbital inclination i, and the two coefficients $u_+ = u_a + u_b$ and $u_- = u_a - u_b$, where u_a, u_b are the quadratic limb-darkening coefficients (Claret 2003, 2004). For the transit fitting, we used the same method as fully described in Barge et al. (2008) and Alonso et al. (2008), with a bootstrap analysis to properly explore the parameter space. We found (Table 2) that the best fit gives values for the two limb-darkening parameters with large error bars, especially for the u_- parameter.

The limb-darkening parameters issue has been already pointed out by various studies carried out using space-based or ground-based observations (Knutson et al. 2007; Southworth 2008). In the case of CoRoT-Exo-3, as the broad *CoRoT* spectral band-pass is unique and not related to any of the photometric filters used for limb-darkening predictions, we decided not to fix the limb-darkening parameters in the transit fitting. We however checked that the values obtained with the best fit model were consistent with the expected theoretical values.

According to Claret (2004) for a given value of $T_{\rm eff}$ and $\log g$, the u_a and u_b values change slightly from one filter to another. As the maximum of transmission of *CoRoT* is close to the V and R bands, we assess the range of predicted values for u_a and u_b respectively, in the B, V, R and i filters. This was done for different values of $T_{\rm eff}$ and $\log g$ which correspond to the physical properties and their uncertainties that we derived for CoRoT-Exo-3 (see Sect. 3.3). As a result, this gives us a range of u_a and u_b predicted values, which simply translates into a range of possible values for both u_- and u_+. We checked that our best fitted values are well within each of these ranges.

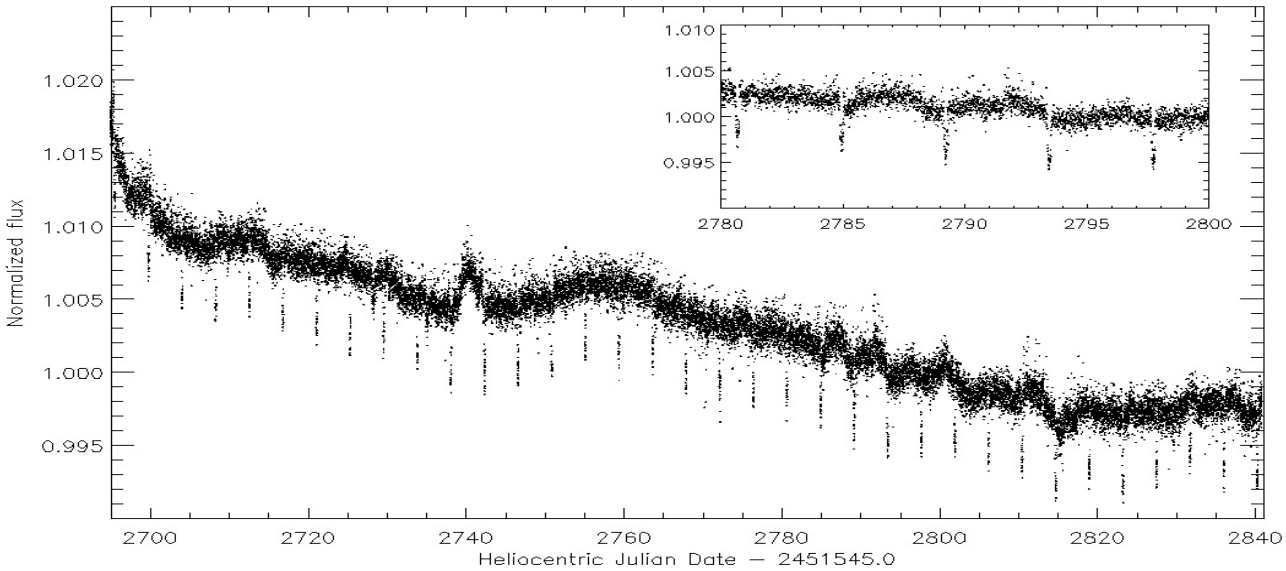

Fig. 1. The 152-days long CoRoT-Exo-3b reduced light curve, binned at a constant time sampling of 512 s and normalized. The low activity level of the star is illustrated in the upper figure which displays a zoomed section of the light curve.

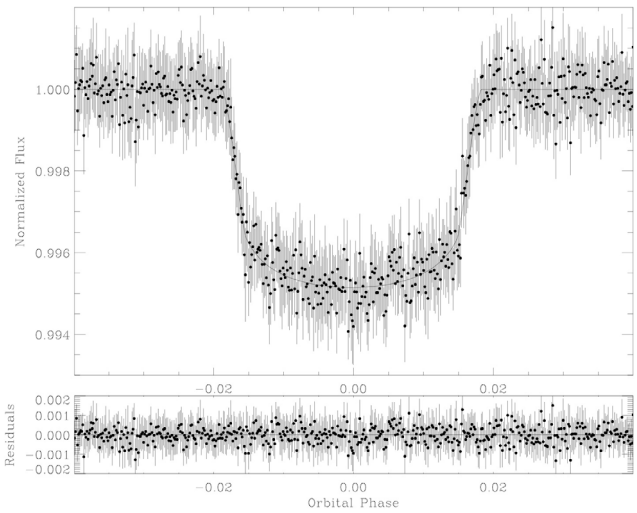

Fig. 2. The phase-folded light curve of the CoRoT-Exo-3b transit with the best fit solution overplotted (solid line). The residuals of the fit are plotted at the bottom of the figure. The rms error is 4.4094×10^{-4} out of eclipse.

It is worth noticing that we found another set of solutions with comparable χ^2 value but at a higher inclination, $i \simeq 89°$. These solutions however give fitted limb-darkening parameters which are even more inconsistent with theoretical ones. As reported by Brown et al. (2001), for transiting planets at low impact parameters, there is a degeneracy in the orbital inclination and the limb darkening coefficients, both effects being difficult to disentangle at the level greater than a few 10^{-4}. We compared the two solutions, and checked at the level of precision we achieve, with a rms error of 4.4×10^{-4} out of transit that they could not be distinguished.

3. Follow-up observations

Ground-based follow-up campaigns of the planet candidates detected by the *alarm mode* in the *CoRoT* light curves from the first long run started in July 2007, or shortly after their detection.

Table 2. Transit parameters derived from the *CoRoT* light curve analyses.

	Best fit all parameters free	
parameter	value	uncertainty
Period (day)	4.25680	±0.000005
T_0 (day)	2 454 283.1383	±0.0003
χ^2	1.020	
θ_1	0.0185	$\pm 1.6 \times 10^{-4}$
$k = R_p/R_\star$	0.0663	$\pm 9.0 \times 10^{-4}$
i (deg)	85.9	±0.8
u_+	0.56	±0.05
u_-	−0.10	±0.07
$M_\star^{1/3}/R_\star$	0.71	±0.04
$a/R_\star$	7.8	±0.4
b $(R_\star)^{(a)}$	0.55	±0.08

$^{(a)}$ Impact parameter.

Such complementary observations are mandatory to identify the nature of the transiting bodies and to further characterize the secured planets. Radial velocity measurements as well as ground-based photometry observations were performed and confirmed the non-stellar nature of the transiting body. High resolution spectra of the host star were later acquired with the *UVES* spectrograph on the VLT.

3.1. Photometric follow-up observations

The relatively large PSF of *CoRoT* (of 20″ × 6″ with the longer axes approximately in N-S direction) and its large aperture masks raise the possibility that any of the nearby fainter stars (see Fig. 3) that contaminate a target lightcurve might in fact be an eclipsing binary mimicking a transit-like signal for the target. Indeed, around CoRoT-Exo-3 there are two such *potential* sources for false alarms, at distances of 5.3 and 5.6″, respectively. As part of the ongoing ground-based photometric follow-up of *CoRoT* candidates, whose motivation and techniques are described in more detail in Deeg et al. (2008, in preparation), time-series imaging was obtained during both

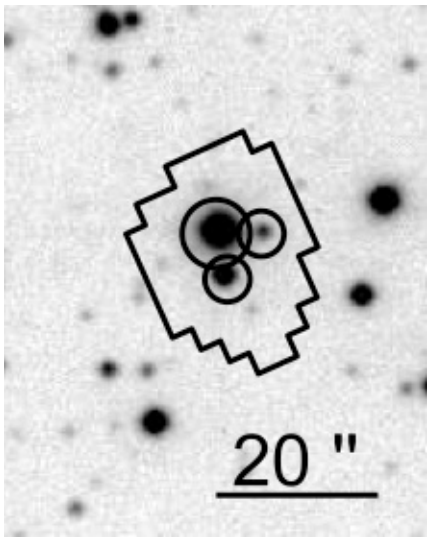

Fig. 3. A CCD image of the field around CoRoT-Exo-3, observed with the IAC80 telescope at a seeing with a FWHM of 1.4″. The largest circle indicates the CoRoT-Exo-3b host star, whereas the smaller circles below and to the right indicate contaminating stars that are 2.9 mag and 4.9 mag fainter, at distances of 5.6″ to the South and 5.3″ to the East, respectively. The irregular shape is the photometric mask used by *CoRoT*. Please note that the East is to the right on the figure.

on-transit and off-transit configurations on separate nights in July and August 2007 with the IAC 80 cm telescope at a spatial resolution of about 1.4″. A comparison of the brightnesses of the transit-candidate as well as of the potential false alarm sources was then performed between the timeseries taken at "on" and "off"-transit configurations. While this comparison could not reproduce *CoRoT*'s observed brightness variation of 5 mmag on the candidate star, the *absence* of any sufficiently large brightness variation (of at least 0.06 and 0.4 mag for the brighter and the fainter of the contaminants, respectively) could be demonstrated. We can therefore deduce that *CoRoT*'s transit-detection arises from a small brightness variation on the target-star itself. Finally, a full transit on the target star was observed at the 1-m *WISE* telescope on 5 July 2008. The shape of the target light curve was consistent with the *CoRoT* light curve, in both transit depth and duration. It nicely confirms the *CoRoT*'s transit detection.

3.2. Radial velocity measurements

In the days following its detection, CoRoT-Exo-3 was observed with the *SOPHIE* spectrograph (Bouchy & The Sophie Team 2006) on the 1.93-m OHP telescope (France). A first set of 5 spectra was recorded between July 28 and August 23, 2007, in high efficiency mode (spectral resolution $R \simeq 40\,000$). Additional measurements were made more than 9 months after, in 2008, in order to investigate a possible drift due to a second companion. The spectra were extracted using the on-line *SOPHIE* reduction pipeline which allows us immediately to perform the radial velocity analysis and thus to rapidly reject false positives. The radial velocities were measured by cross-correlation of the reduced spectra with a numerical G2 mask, constructed from the Sun spectrum atlas including up to 3645 lines. Nearly at the same dates, the star was observed with the Coudé échelle spectrograph of the 2-m-Alfred Jensch telescope in Tautenburg, Germany (*TLS*). In three different nights, two spectra were recorded, each of 30 min exposure time. Using the so-called VIS grism and a slit width of 2″, these spectra cover the wavelength range from 470 to 740 nm at a resolution of $\lambda/\Delta\lambda = 33\,000$, giving about 4 pixels per resolution element. Moonlight was removed by taking a spectrum of the moon, scaled to the level measured along the 30″ long slit and then subtracting it. For flat-fielding we used a specially designed dome-flat utility, and for the wavelength calibration a ThAr-lamp. The spectra were bias-subtracted, flat-fielded, cosmic rays removed and extracted using standard IRAF routines. After accounting for an instrumental shift using the telluric lines, the radial velocity of the star was finally measured by cross-correlating the spectrum with the radial velocity standard star HR 5777 for which we used a radial velocity of +49.12 ± 0.06 km s^{-1} (Murdoch et al. 1993). For the cross-correlation, we masked out parts of the spectrum contaminated by telluric lines. Although the star appeared as a fast rotator with a $v \sin i$ value of about 17 km s^{-1}, these first radial velocity measurements allowed us to confirm the planetary nature of the transiting body.

Four complementary measurements were carried out with the *HARPS* spectrograph on the 3.6 m telescope (La Silla, Chile) in order to perform the line-bisector analysis to look for asymmetries in the spectral line profiles, as could be caused by contamination from an unresolved eclipsing binary (Queloz et al. 2001). Four exposures of 30 min each were recorded over four consecutive nights covering one orbital period. Eighteen additional measurements were carried out with the *CORALIE* spectrograph on the Euler 1.2-m telescope. *CORALIE* has recently been upgraded, as described in Wilson et al. (2008), in order to follow-up *CoRoT* targets up to 14th magnitude.

Further spectra were collected at McDonald Observatory (Texas, USA) during three nights on May 2008 in order to investigate a possible drift in the radial velocity. The Sandiford echelle spectrograph mounted at the Cassegrain focus of the 2.1 m Otto Struve telescope was used in conjunction with a 1″ slit. The configuration yielded a spectral coverage of 5070−6050 Å at a resolving power $R = 60\,000$. Two consecutive spectra of 30 min were obtained during each night and with calibration spectra acquired before and after each stellar observation. Spectral order extraction followed standard procedures under the IRAF environment. HR 5777 was used as the standard star for the radial velocity cross-correlation.

The complete radial velocity measurements obtained with these five spectrographs are presented in Table 3. The five sets of relative radial velocities were simultaneously fitted with a Keplerian model, with the epoch of the transit being fixed at the *CoRoT* value and with an adjusted offset between the different instruments. No significant eccentricity was found and we decided to set it to zero. The best fit parameters yields $K = 2.194$ km s^{-1} ± 0.027. Figure 4 shows all the radial velocity measurements after subtracting the individual offsets and phase folded to the orbital period.

A line-bisector analysis is routinely done for each *CoRoT* candidate in order to identify the presence of any spatially unresolved stellar companion which could be the source of the radial velocity variation. This analysis performed on the 4 *HARPS* measurements of our target does not show any significant variation (see Fig. 5) thus excluding a blend scenario due to an unresolved eclipsing binary. Several *CORALIE* measurements were made during the transit but the Rossiter-McLaughlin effect was not detected. Indeed, considering the planet-star radius ratio of 0.066 and the rotational velocity of $v \sin i$ of 17 km s^{-1}, the expected semi-amplitude of the radial velocity anomaly for a central and spin-aligned transit is only 55 m s^{-1}. This is well below

Table 3. Radial velocity measurements for CoRoT-Exo-3b.

HJD	exp time (s)	$v_{\rm rad}$ km s^{-1}	$\sigma v_{\rm rad}$ km s^{-1}	Spectrograph
2 454 309.5696	3600	−58.262	0.046	*SOPHIE*
2 454 316.4672	2700	−54.269	0.060	*SOPHIE*
2 454 317.4443	3000	−57.122	0.060	*SOPHIE*
2 454 318.3674	3000	−58.371	0.078	*SOPHIE*
2 454 336.4002	2700	−55.938	0.047	*SOPHIE*
2 454 590.6002	3600	−58.386	0.051	*SOPHIE*
2 454 643.5273	2700	−54.386	0.074	*SOPHIE*
2 454 331.3590	3600	−57.130	0.250	*TLS*
2 454 332.3600	3600	−54.460	0.290	*TLS*
2 454 336.9060	3600	−53.650	0.240	*TLS*
2 454 341.6815	1800	−53.978	0.052	*HARPS*
2 454 342.6366	1800	−55.867	0.049	*HARPS*
2 454 343.6556	1800	−58.331	0.054	*HARPS*
2 454 344.6816	1800	−56.683	0.057	*HARPS*
2 454 320.7188	3600	−54.628	0.200	*CORALIE*
2 454 322.7074	3600	−58.523	0.198	*CORALIE*
2 454 330.6931	3600	−58.457	0.141	*CORALIE*
2 454 372.4932	3600	−56.263	0.172	*CORALIE*
2 454 372.5133	3600	−56.597	0.186	*CORALIE*
2 454 372.5281	3600	−56.565	0.218	*CORALIE*
2 454 372.5429	3600	−56.644	0.170	*CORALIE*
2 454 372.5629	3600	−56.535	0.189	*CORALIE*
2 454 372.5829	3600	−57.039	0.210	*CORALIE*
2 454 372.6032	3600	−57.154	0.221	*CORALIE*
2 454 372.6231	3600	−57.265	0.259	*CORALIE*
2 454 372.6433	3600	−56.951	0.214	*CORALIE*
2 454 379.5247	3600	−54.772	0.178	*CORALIE*
2 454 380.5267	3600	−55.498	0.192	*CORALIE*
2 454 387.5000	3600	−56.494	0.217	*CORALIE*
2 454 388.5207	3600	−54.844	0.226	*CORALIE*
2 454 394.5333	3600	−58.696	0.211	*CORALIE*
2 454 400.5461	3600	−55.556	0.232	*CORALIE*
2 454 607.8861	3600	−57.786	0.163	SANDIFORD
2 454 609.8528	3600	−53.187	0.100	SANDIFORD
2 454 613.8684	3600	−53.308	0.157	SANDIFORD

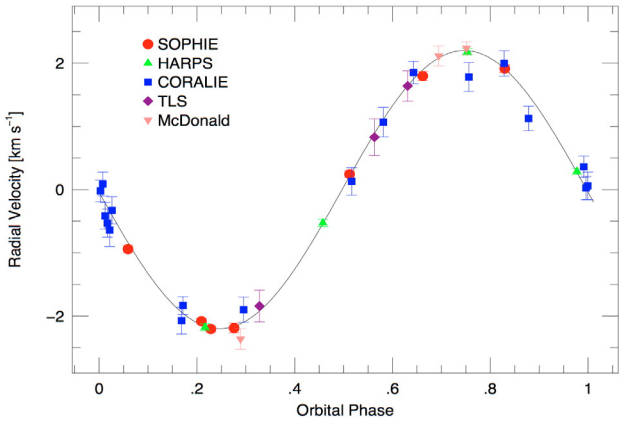

Fig. 4. The phase-folded radial velocity measurements from the different spectrographs used for the follow-up campaign, with the best fit solution over-plotted (solid line).

the *CORALIE* radial velocity uncertainties of ~200 m s^{-1}; a further such measurement with *HARPS* is going to be carried out.

In total, the radial velocity measurements cover a duration of more than 11 months, five additional measurement recently made on Spring 2008 (Fig. 6). No significant drift was detected over this period, excluding the presence of an additional massive companion (>2 $M_{\rm Jup}$) with a period less than 11 months.

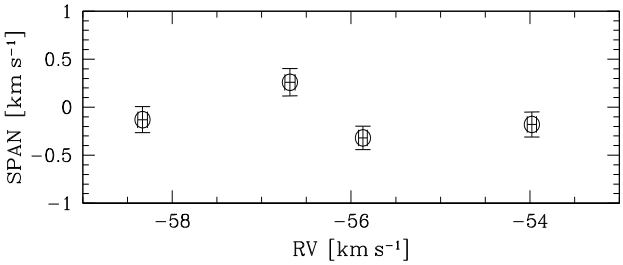

Fig. 5. The bisector span, giving the differences in radial velocities between top and bottom of a bisector, as a function of radial velocity, measured with *HARPS*.

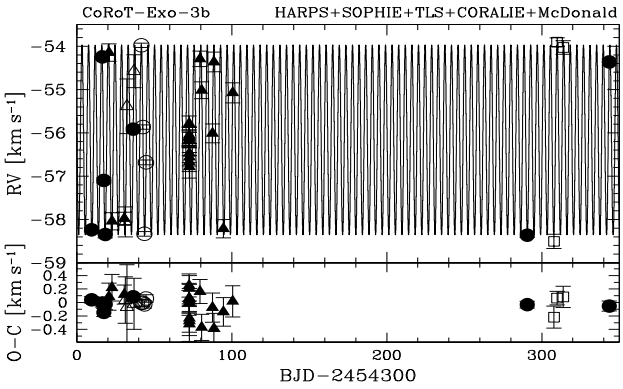

Fig. 6. The complete set of radial velocity measurements over a one year period: *SOPHIE* (black circle), *TLS* (open triangle), *HARPS* (open circle), *CORALIE* (black triangle) and *SANDIFORD* (open square) spectrographs.

Considering the projected rotation velocity $v \sin i$ of 17 ± 1 km s^{-1} and assuming that the rotation axis of the star is perpendicular to the line-of-sight, the star is rotating in 4.6 ± 0.4 days. Given the relatively large mass and short period of the companion, one might expect it to have synchronized the rotation of its host star to its orbital period via tidal interaction (Dobbs-Dixon et al. 2004; Jackson et al. 2008). The observed rotational velocity of the star is indeed compatible with this hypothesis and the phenomenon has recently been reported for two other massive planets orbiting an F-star in circular orbit: τ Boo (Donati et al. 2008) and CoRoT-Exo-4b (Aigrain et al. 2008). We attempted to measure the photometric rotation period of the star from the out-of-transit light curve, using a discrete autocorrelation function (ACF) method as was successfully done for CoRoT-Exo-4b (Aigrain et al. 2008). However, no significant signal was detected, even when computing the ACF using only the second half of the light curve, where the photometric variability is slightly more pronounced. It appears that the star is not sufficiently active to sustain coherent active regions producing detectable rotational modulation over more than one period.

3.3. High resolution spectroscopy

The *SOPHIE* and *HARPS* spectra were of too poor a quality to allow a proper spectral analysis. Consequently, the star was observed with the *UVES* spectrograph at the end of October 2007. Two exposures of 2380 s each were recorded, using the a spectrometer slit of 0.7″ which yielded a resolving power of ≃65 000. The co-added spectra gives a S/N ratio greater than 140 per resolution element over the entire spectral range.

Table 4. CoRoT-Exo-3 parameters derived from radial velocity and spectroscopic analyses.

$v_{\rm rad}$ (km s^{-1})	−56.162	±0.016
$v_{\rm rot} \sin i$ (km s^{-1})	17.0	±1.0
$T_{\rm eff}$	6740 K	±140
log g	4.22$^{(a)}$	±0.07
log g	4.25$^{(b)}$	±0.07
[M/H]	−0.02	±0.06
Spectral type	F3 V	
$M_\star$	1.37	±0.09
$R_\star$	1.56	±0.09
Age	1.6−2.8 Gyr	
Distance	680 pc	±160

$^{(a)}$ Determined from the spectroscopic analysis; $^{(b)}$ determined using evolutionary models and the light-curve $M_\star^{1/3}/R_\star$ parameter.

The spectral analysis was performed using different methods and by different *CoRoT* teams in an independent way. Some of the methods consist of spectral synthesis modeling, using a library of synthetic spectra, as presented in Barge et al. (2008). In particular, we used the Spectroscopy Made Easy (SME 2.1) package (Valenti & Piskunov 1996; Valenti & Fischer 2005). Other methods are based on equivalent width measurements of isolated lines, while the semi-automatic software package VWA (Bruntt et al. 2002, 2008) performs iterative fitting of calculated synthetic spectra. These methods required a careful normalization of the spectra. This was done order per order by fitting a spline function to the continuum windows identified in a synthetic spectrum and calculated with parameters close to those of the target star. We made sure that the shape and depth of lines in adjacent spectral orders were in agreement. In the final spectrum the orders were merged and the overlapping parts were weighted by the S/N. We found that the estimated values of the atmospheric parameters: effective temperature ($T_{\rm eff}$), surface gravity (log g) and metallicity ([M/H]), obtained by the different methods agreed within the estimated errors. The adopted values are listed in Table 4.

As part of the analysis we adjusted the macroturbulence to fit the wings of the spectral lines and found $v_{\rm macro}$ = 4.0 ± 0.6 km s^{-1}. The rotational broadening was found to be 17 ± 1 km s^{-1}.

The detailed abundance results we report here are based on the VWA method. We used 192 mostly non-blended lines and the abundances were calculated relative to the solar spectrum from Hinkle et al. (2000), following the approach by Bruntt et al. (2008). Using the fundamental parameters listed in Table 4 for the atmospheric model, we determined the abundances of 17 individual elements as listed in Table 5.

The uncertainty on the abundances includes a contribution of 0.06 dex due to the uncertainty on the fundamental parameters. The overall metallicity is found as the mean abundance of the elements with at least 5 lines, that is Ca, Ti, Cr, Fe and Ni, giving [M/H] = −0.02 ± 0.06 (Fig. 7). We did not include Mn since it has a significantly lower abundance than the other metals. It is worth noticing that we found no evidence for the star being chemically peculiar. Our target star is slightly cooler than 7000 K ($T_{\rm eff}$ = 6740 K) and departure from LTE is expected. Rentzsch-Holm (1996) investigated the NLTE effects for Fe in A-type stars with $T_{\rm eff}$ > 7000 K. We extrapolated from her Fig. 4 for solar metallicity to find a first-order correction [Fe I/H]$_{\rm NLTE}$ = [Fe I/H]$_{\rm LTE}$ + 0.05. This value has been added to Fe I in Table 5. The abundances found from Fe II lines are essentially unaffected.

Table 5. Abundances of 17 elements in CoRoT-Exo-3.

Element	log $N/N_{\rm tot}$	Number of lines
C I	−0.40	1
Na I	−0.14	2
Mg I	−0.08	1
Si I	−0.03(0.07)	3
Ca I	+0.03(0.07)	5
Sc II	−0.11(0.08)	4
Ti I	−0.01(0.08)	8
Ti II	+0.02(0.06)	5
V I	−0.36	2
Cr I	−0.09(0.11)	5
Cr II	−0.06(0.07)	5
Mn I	−0.26(0.08)	7
Fe I$^{(a)}$	+0.03(0.06)	92
Fe II	+0.02(0.06)	13
Co I	+0.04	2
Ni I	−0.06(0.06)	29
Cu I	−0.66	1
Zn I	−0.18	1
Y II	−0.07(0.20)	4
Zr II	−0.15	2

$^{(a)}$ Corrected for non-LTE effects.

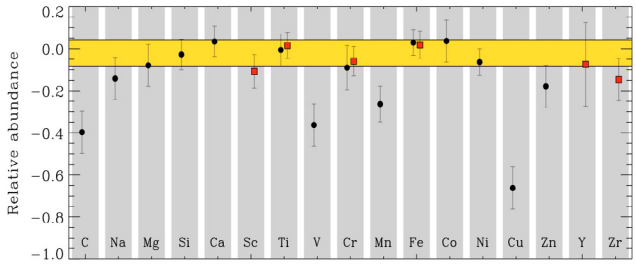

Fig. 7. Abundances of the elements measured in CoRoT-Exo-3. Black circles are for neutral elements and box symbols are used for ionized ones. The metallicity and the 1-σ uncertainty range are indicated by the horizontal yellow bar.

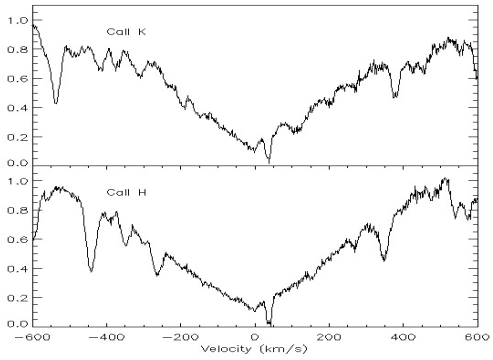

Fig. 8. The Ca II H & K lines observed in the *UVES* spectra of CoRoT-Exo-3. No emission feature is seen is the core of the stellar lines. The velocity scale is in the rest frame of the star.

To make the atmosphere model produce the same result for neutral and ionized Fe lines, log g was increased by 0.10 dex.

Inspection of the spectra reveals no emission in the Ca II H and K lines (Fig. 8) or other photospheric lines. This is in good agreement with the lack of photometric variation in the light curve, as well as with no strong jitter in the radial velocity measurements.

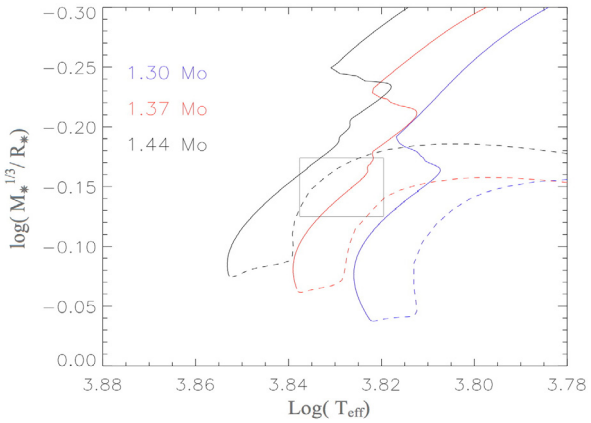

Fig. 9. Stellar evolutionary tracks from the STAREVOL models for masses in the range 1.30 to 1.44 $M_{\odot}$ for the measured metallicity [M/H] = −0.02, shown with the parameters derived from the observations: $T_{\rm eff}$ and $M_{\star}^{1/3}/R_{\star}$.

To determine the mass and radius of the parent star we used the same methodology as for the two first *CoRoT* planets (Barge et al. 2008; Bouchy et al. 2008), i.e. we used $T_{\rm eff}$ and [M/H] from the spectroscopic analysis and $M_{\star}^{1/3}/R_{\star}$ from the light curve analysis which provides a better estimate of the fundamental parameters, thanks to the good quality of the *CoRoT* light curve. From a comparison with evolutionary models as shown in Fig. 9, we can constrain the fundamental parameters of the parent star. In this study, we mainly relied on *STAREVOL* (Siess 2006; Palacios, private communication) stellar evolution models to derive the stars precise parameters. We also compared these with the results obtained using *CESAM* (Morel & Lebreton 2007) and we found that both stellar evolution model tracks were in agreement. The details of the comparison between the different models will be presented in a forthcoming paper. We find the stellar mass to be $M_{\star} = 1.37 \pm 0.09\ M_{\odot}$ and the stellar radius $R_{\star} = 1.56 \pm 0.09\ R_{\odot}$, with an age in the range 1.6−2.8 Gyr. This infers a surface gravity of $\log g = 4.24 \pm 0.07$, which is in good agreement with the spectroscopic result of $\log g = 4.22 \pm 0.07$, and implies that the correction due to NLTE effects is indeed relevant.

In a final step, we calculated the distance to the star. We used the physical parameters of the star we derived and its colors to estimate the reddening. Using the extinction law from Rieke & Lebofsky (1985), we found the absorption $A_V = 0.52 \pm 0.5$ mag, yielding a distance of 680 ± 160 pc. We checked that the value of the extinction we derived is consistent with strong saturated Na I (D1) and (D2) interstellar lines as well as reddening maps of Schlegel et al. (1998) which give a maximum absorption towards our target of 1 mag.

We also investigated the possibility of a physical association between CoRoT-Exo-3 and the nearby brightest companion at 5.6″. Given our estimated distance to the star, the range of possible extinction on the line of sight, and the apparent visual magnitude of the contaminant ($V = 16.46 \pm 0.07$) we derived an absolute visual magnitude $M_V = 6.8 \pm 0.5$, consistent with a K-type star. We compared the colors of the contaminant we calculated from our ground-based observations and *2-MASS* photometry (Table 1) with those predicted for a star of this spectral type. We found that within the precision of the different parameters, a physical association could not be excluded. In that case, their separation would be about 3800 AU and the orbital period of the companion would be ∼235 000 years. On the other hand, according to the *UCAC2* catalogue (Zacharias et al. 2004), CoRoT-Exo-3 displays a proper motion while none is detected for the companion. This non detection would hence rather favor a background star. Given our current knowledge we can not draw a firm conclusion about the possibility of binarity for CoRoT-Exo-3. More complementary observations are required.

Table 6. CoRoT-Exo-3b parameters.

Mass ($M_{\rm Jup}$)	21.66 ± 1.0
Radius ($R_{\rm Jup}$)	1.01 ± 0.07
density (g cm^{-3})	26.4 ±5.6
log g	4.72 ± 0.07

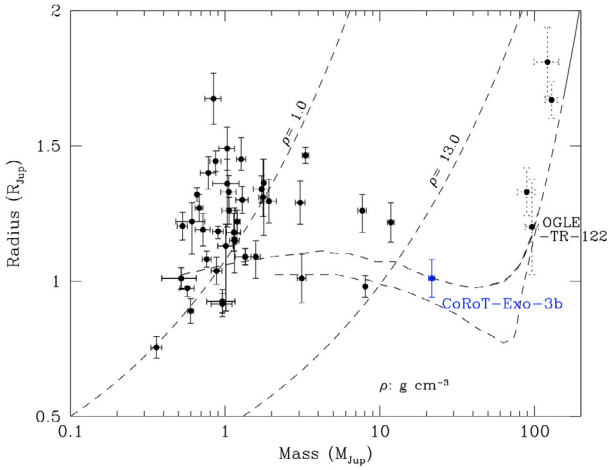

Fig. 10. Mass-radius diagram for all transiting planets and low-mass M stars with theoretical isochrones at 10 and 1 Gyr from Baraffe et al. (2003) overplotted.

4. CoRoT-exo-3b parameters and discussion

4.1. Nature of CoRoT-exo-3b

Using the stellar properties determined in the previous section and the characteristics of the transiting body as derived from the transit and the radial velocity fits, we derive a mass of the companion of $M_p = 21.66 \pm 1.0\ M_{\rm Jup}$, a radius $R_p = 1.01 \pm 0.07\ R_{\rm Jup}$, an inferred density of $\rho = 26.4 \pm 5.6$ g cm^{-3}, and a surface gravity of $\log g = 4.72 \pm 0.07$ (Table 6). With such properties, CoRoT-Exo-3b clearly distinguishes itself from the regular close-in extrasolar planet population. In a mass-radius diagram, the position of CoRoT-Exo-3b is well inside the gap in mass between planetary and low-mass star companions (Fig. 10).

Traditionally, a planet has been defined as an object lighter than 13 $M_{\rm Jup}$, as such objects are supposed not to have an internal nuclear source of energy (Deuterium burning). From this point of view, CoRoT-Exo-3b is definitely a brown-dwarf. Indeed, in this low mass range, models predict an almost constant Jupiter-size radius (Baraffe et al. 2003). As illustrated in Fig. 10, CoRoT-Exo-3b parameters are in good agreement with the expected mass-radius relationship on the low-mass tail of these substellar objects.

Another definition makes use of the formation scenario: a planet is formed by core accretion of dust/ices in a protoplanetary disk, while a brown-dwarf is formed by collapse of a dense molecular gas cloud. In that case, the separation between the brown-dwarf and planet population is blurrier since a planet, starting with a solid core, can end up with a gaseous envelope as

massive as a few tens of Jupiter masses. Recent improvements of the core-accretion models predict the formation of a wide variety of giant planets (Alibert et al. 2005) with masses up to 10 $M_{\rm Jup}$, depending on the initial conditions. Some authors (Mordasini et al. 2007) even suggested that the mass of these "superplanets" could be as high as 25 $M_{\rm Jup}$. An alternative hypothesis for the origin of such massive planetary bodies could be collisions between several massive planets, as recently proposed by Baraffe et al. (2008).

CoRoT-Exo-3b could be considered either as a member of a new population of very massive planets, or "superplanets", or a representative of the low-mass part of the brown-dwarf family.

4.2. Is CoRoT-Exo-3b exceptional?

The discovery of a 21 $M_{\rm Jup}$ object in a short period orbit is unexpected given the paucity of objects in the so-called "brown-dwarf desert" (e.g. Halbwachs et al. 2000; Grether & Lineweaver 2006). However, Doppler surveys have found companions to HD 41004B (Zucker et al. 2004) and HD 162020 (Udry et al. 2002) that bear some similarities with CoRoT-Exo-3b with a minimum masses between 10 and 20 $M_{\rm Jup}$ and short orbital periods. Nevertheless, it is difficult to assess the statistical significance of the lack of short period companions with masses between 10 and 20 $M_{\rm Jup}$ detected from the radial velocity surveys. For the very large (over 20 000 stars) Doppler mid-accuracy survey made by *CORAVEL* (Nordström et al. 2004), the lack of sensitivity may have prevented these surveys from detecting such companions orbiting fast rotating stars. Accurate Doppler planet surveys, based on a much larger and complete sample, like the one carried out with *CORALIE* (Udry et al. 2000) would have the capability to detect a companion like CoRoT-Exo-3b. However, in that case, the observing strategy is focused on slow rotators. The significant rotational line broadening would have affected the search strategy, either by removing these objects after one measurement or by setting them aside with a very low observation ranking priority. This selection bias towards slow rotators may now become remedied, thanks to recent studies aiming at enlarging the space of parameters for host stars (e.g. Galland et al. 2005).

4.3. Do massive companions require massive stars?

Among the 46 well characterized transiting planets, 19 are orbiting a star with a mass ≥1.1 $M_{\odot}$, as illustrated in Fig. 11. It is worth noticing that the three most massive planets so far discovered are orbiting F-type stars: HAT-P-2b (Bakos et al. 2007) with mass of 8.6 $M_{\rm Jup}$ orbits a F8 star, WASP-14b (Joshi et al. 2008) and XO-3b (Johns-Krull et al. 2008) with masses of 7.77 $M_{\rm Jup}$ and 11.79 $M_{\rm Jup}$ respectively, both orbiting F5-type stars. Although the sample is still very limited, it suggests that the close-orbiting companions to host stars with mass above 1.1 $M_{\odot}$ could be more massive than companions to lower mass hosts. In that case, we could not exclude that the brown-dwarf desert is not that dry around F-type stars.

Alternatively, the discovery of companions in short periodic orbits with masses between 5 and 20 $M_{\rm Jup}$ could be suggestive of a different formation mechanism. The mass distribution of planet companions in short period orbits found by radial velocity surveys on solar type stars becomes sparsely populated for masses beyond 3 $M_{\rm Jup}$ (Fig. 12). Below 3 $M_{\rm Jup}$ the planet population is steeply rising as a function of decreasing planet mass. In a mass distribution diagram these massive planets look

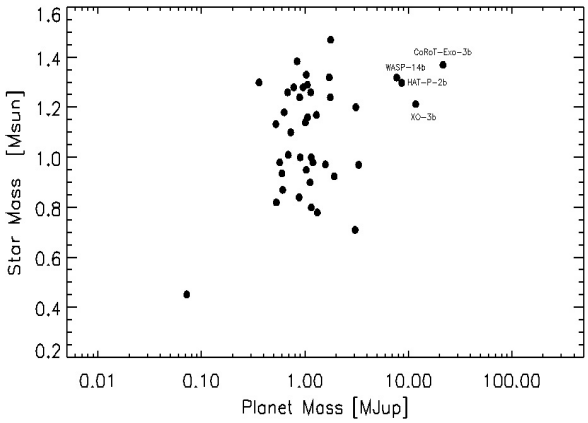

Fig. 11. Mass of the known transiting extrasolar planets with orbital period less than 10 days, as a function of the mass of their parent star.

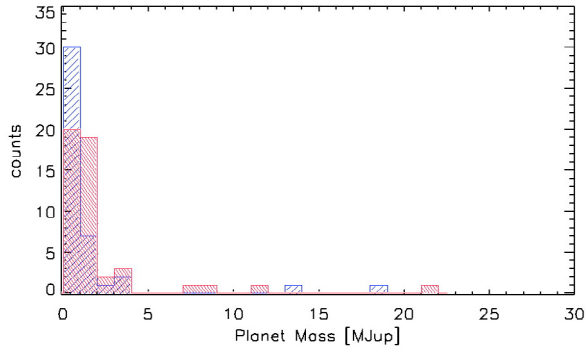

Fig. 12. Mass distribution of close-in planets. Blue: planets with orbital period less than 30 days, detected by radial velocity and with a minimum mass estimate only; red: transiting planets.

clearly off the short tail of the planet distribution. Different formation mechanism for massive planets on short orbits have already been pointed out by Udry et al. (2002), who noticed that they seem to be always found in binary systems. In the case of CoRoT-Exo-3, more investigations may be necessary to establish unambiguously whether the star belongs to a binary system or not. If one compares the bulk of Doppler planets with the metallicity distribution of HAT-P-2, WASP-14, XO-3 and CoRoT-Exo-3, it is interesting to point out that it is not skewed towards metal rich stars, as one would expect for such planets (Udry & Santos 2007), suggesting again possibly a different formation mechanism. Therefore one might conclude that CoRoT-Exo-3b could be different from the bulk of extrasolar planets found by Doppler surveys but not from the few companions with masses above 3 $M_{\rm Jup}$. On the other hand, we note that HAT-P2b, WASP-14b and XO-3b are all in eccentric orbits, but not CoRoT-Exo-3b. Considering the strong tidal interactions of massive close-in companions with their central star, this suggests an extra body that may have brought – and maintained – these planets in their current orbit; something that is not valid for CoRoT-Exo-3b, and whose formation history might therefore be of different nature.

5. Conclusion

After more than one decade of intensive ground-based extrasolar planet hunting, *CoRoT* has detected and measured, thanks to the support of ground-based facilities, the fundamental parameters of a massive close-in companion object, located at the

overlapping region between the planet and the brown-dwarf domains. CoRoT-Exo-3b reopens the debate about the existence of a hitherto non-detected brown-dwarf population at short orbital periods but also about the definition of a planet, such as the common one which, in this range of mass, relies on the deuterium burning limit. The exact nature of this new object is therefore still doubtful. Its parameters are in pretty good agreement with the model predictions for brown-dwarfs. If that is that case, it might simply be the first secure and well-characterized object at the lowest mass end of the stellar population. If CoRoT-Exo-3b is indeed a brown-dwarf one should review as well the other massive planets like XO-3b, HAT-P2b and WASP-14b as potential members of this class. An alternative explanation is that CoRoT-Exo-3b belongs to a new, yet unexplored, very massive planet population, widening the variety of exoplanets. The currently ambiguous nature of CoRoT-Exo-3b makes it therefore a very worthwhile object for further deeper studies.

Acknowledgements. H.J.D. and J.M.A. acknowledge support by grants ESP2004-03855-C03-03 and ESP2007-65480-C02-02 of the Spanish Education and Science Ministry. R.A. acknowledges support by grant CNES-COROT-070879. The German CoRoT Team (TLS and Univ. Cologne) acknowledges DLR grants 50OW0204, 50OW0603, 50QP07011. Some of the data published in this article were acquired with the IAC80 telescope operated by the Instituto de Astrofísica de Tenerife at the Observatorio del Teide. The building of the input *CoRoT*/Exoplanet catalog was made possible thanks to observations collected for years at the Isaac Newton Telescope (INT), operated on the island of La Palma by the Isaac Newton group in the Spanish Observatorio del Roque de Los Muchachos of the Instituto de Astrofisica de Canarias. The SME 2.1 package was kindly made available by N. Piskunov and J. Valenti.

References

Aigrain, S., Collier Cameron, A., Ollivier, M., et al. 2008, A&A, 488, L43
Alibert, Y., Mordasini, C., Benz, W., & Winisdoerffer, C. 2005, A&A, 434, 343
Alonso, R., Auvergne, M., Baglin, A., et al. 2008, A&A, 482, L21
Bakos, G. Á., Shporer, A., Pál, A., et al. 2007, ApJ, 671, L173
Baraffe, I., Chabrier, G., Barman, T. S., Allard, F., & Hauschildt, P. H. 2003, A&A, 402, 701
Baraffe, I., Chabrier, G., & Barman, T. 2008, A&A, 482, 315
Barge, P., Baglin, A., Auvergne, M., et al. 2008, A&A, 482, L17
Bouchy, F., & The Sophie Team 2006, in Tenth Anniversary of 51 Peg-b: Status of and prospects for hot Jupiter studies, ed. L. Arnold, F. Bouchy, & C. Moutou, 319
Bouchy, F., Queloz, D., Deleuil, M., et al. 2008, A&A, 482, L25
Brown, T. M., Charbonneau, D., Gilliland, R. L., Noyes, R. W., & Burrows, A. 2001, ApJ, 552, 699
Bruntt, H., Catala, C., Garrido, R., et al. 2002, A&A, 389, 345
Bruntt, H., De Cat, P., & Aerts, C. 2008, A&A, 478, 487
Claret, A. 2003, A&A, 401, 657
Claret, A. 2004, A&A, 428, 1001
Deleuil, M., Meunier, J. C., Moutou, C., et al. 2008, AJ, submitted
Dobbs-Dixon, I., Lin, D. N. C., & Mardling, R. A. 2004, ApJ, 610, 464
Donati, J.-F., Moutou, C., Farès, R., et al. 2008, MNRAS, 385, 1179
Galland, F., Lagrange, A.-M., Udry, S., et al. 2005, A&A, 443, 337
Giménez, A. 2006, A&A, 450, 1231
Grether, D., & Lineweaver, C. H. 2006, ApJ, 640, 1051
Halbwachs, J. L., Arenou, F., Mayor, M., Udry, S., & Queloz, D. 2000, A&A, 355, 581
Hinkle, K., Wallace, L., Valenti, J., & Harmer, D. 2000, Visible and Near Infrared Atlas of the Arcturus Spectrum 3727−9300 Å, ed. K. Hinkle, L. Wallace, J. Valenti, & D. Harmer (San Francisco: ASP)
Jackson, B., Greenberg, R., & Barnes, R. 2008, ApJ, 681, 1631
Johns-Krull, C. M., McCullough, P. R., Burke, C. J., et al. 2008, ApJ, 677, 657
Joshi, Y. C., Pollacco, D., Collier Cameron, A., et al. 2008, ArXiv e-prints, 806
Knutson, H. A., Charbonneau, D., Noyes, R. W., Brown, T. M., & Gilliland, R. L. 2007, ApJ, 655, 564
Mordasini, C., Alibert, Y., Benz, W., & Naef, D. 2007, ArXiv e-prints, 710
Morel, P., & Lebreton, Y. 2007, Ap&SS, 460
Murdoch, K. A., Hearnshaw, J. B., & Clark, M. 1993, ApJ, 413, 349
Nordström, B., Mayor, M., Andersen, J., et al. 2004, A&A, 418, 989
Pinheiro da Silva, L., Rolland, G., Lapeyrere, V., & Auvergne, M. 2008, MNRAS, 384, 1337
Queloz, D., Henry, G. W., Sivan, J. P., et al. 2001, A&A, 379, 279
Quentin, C., Barge, P., Cautain, R., et al. 2006, in ESA SP, 1306, 409
Rentzsch-Holm, I. 1996, A&A, 312, 966
Rieke, G. H., & Lebofsky, M. J. 1985, ApJ, 288, 618
Schlegel, D. J., Finkbeiner, D. P., & Davis, M. 1998, ApJ, 500, 525
Siess, L. 2006, A&A, 448, 717
Southworth, J. 2008, MNRAS, 386, 1644
Surace, C., Alonso, R., Barge, P., et al. 2008, SPIE, 7019, 132
Udry, S., & Santos, N. C. 2007, ARA&A, 45, 397
Udry, S., Mayor, M., Naef, D., et al. 2000, A&A, 356, 590
Udry, S., Mayor, M., Naef, D., et al. 2002, A&A, 390, 267
Valenti, J. A., & Fischer, D. A. 2005, VizieR Online Data Catalog, 215, 90141
Valenti, J. A., & Piskunov, N. 1996, A&AS, 118, 595
Wilson, D. M., Gillon, M., Hellier, C., et al. 2008, ApJ, 675, L113
Zacharias, N., Urban, S. E., Zacharias, M. I., et al. 2004, AJ, 127, 3043
Zucker, S., Mazeh, T., Santos, N. C., Udry, S., & Mayor, M. 2004, A&A, 426, 695

[1] Laboratoire d'Astrophysique de Marseille (UMR 6110), Technopole de Marseille-Étoile, 13388 Marseille Cedex 13, France
e-mail: magali.deleuil@oamp.fr
[2] Instituto de Astrofísica de Canarias, C. via Lactea S/N, 38200 La Laguna, Spain
[3] Institut d'Astrophysique de Paris, UMR7095 CNRS, Université Pierre & Marie Curie, 98bis Bd Arago, 75014 Paris, France
[4] LESIA, CNRS UMR 8109, Observatoire de Paris, 5 place J. Janssen, 92195 Meudon, France
[5] School of Physics, University of Exeter, Stocker Road, Exeter EX4 4QL, UK
[6] School of Physics A28, University of Sydney, Australia
[7] IAS, Université Paris XI, 91405 Orsay, France
[8] School of Physics and Astronomy, University of St Andrews, UK
[9] Institute of Planetary Research, DLR, Rutherfordstr. 2, 12489 Berlin, Germany
[10] Observatório Nacional, Rio de Janeiro, RJ, Brazil
[11] Institute for Astronomy, University of Vienna, Türkenschanzstrasse 17, 1180 Vienna, Austria
[12] Research and Scientific Support Department, European Space Agency, ESTEC, 2200 Noordwijk, The Netherlands
[13] Thüringer Landessternwarte Tautenburg, Sternwarte 5, 07778 Tautenburg, Germany
[14] Observatoire de Genève, Université de Genève, 51 Ch. des Maillettes, 1290 Sauverny, Switzerland
[15] Observatoire de la Côte d'Azur, Laboratoire Cassiopée, CNRS UMR 6202, BP 4229, 06304 Nice Cedex 4, France
[16] Space Research Institute, Austrian Academy of Sciences, Schmiedlstrasse 6, 8042 Graz, Austria
[17] School of Physics and Astronomy, R. and B. Sackler Faculty of Exact Sciences, Tel Aviv University, Tel Aviv 69978, Israel
[18] Rheinisches Institut für Umweltforschung, Universität zu Köln, Abt. Planetenforschung, Aachener Str. 209, 50931 Köln, Germany
[19] Center for Astronomy and Astrophysics, TU Berlin, Hardenbergstr. 36, 10623 Berlin, Germany
[20] LUTH, Observatoire de Paris-Meudon, 5 place J. Janssen, 92195 Meudon, France